



Threshold regulation and stochasticity from the MecA/ClpCP proteolytic system in *Streptococcus mutans* competence

M. Son,¹ J. Kaspar,² S. J. Ahn,² R. A. Burne ² and S. J. Hagen ^{1††}

¹Department of Physics, University of Florida, Gainesville, FL 32611, USA.

²Department of Oral Biology, University of Florida, Gainesville, FL 32610, USA.

Summary

Many bacterial species use the MecA/ClpCP proteolytic system to block entry into genetic competence. In *Streptococcus mutans*, MecA/ClpCP degrades ComX (also called SigX), an alternative sigma factor for the *comY* operon and other late competence genes. Although the mechanism of MecA/ClpCP has been studied in multiple *Streptococcus* species, its role within noisy competence pathways is poorly understood. *S. mutans* competence can be triggered by two different peptides, CSP and XIP, but it is not known whether MecA/ClpCP acts similarly for both stimuli, how it affects competence heterogeneity, and how its regulation is overcome. We have studied the effect of MecA/ClpCP on the activation of *comY* in individual *S. mutans* cells. Our data show that MecA/ClpCP is active under both XIP and CSP stimulation, that it provides threshold control of *comY*, and that it adds noise in *comY* expression. Our data agree quantitatively with a model in which MecA/ClpCP prevents adventitious entry into competence by sequestering or intercepting low levels of ComX. Competence is permitted when ComX levels exceed a threshold, but cell-to-cell heterogeneity in MecA levels creates variability in that threshold. Therefore, MecA/ClpCP provides a stochastic switch, located downstream of the already noisy *comX*, that enhances phenotypic diversity.

Introduction

Many species of streptococci can become naturally transformable by entering the transient physiological state known as genetic competence (Johnston *et al.*, 2014; Fontaine *et al.*, 2015). Competence plays a particularly important role for the oral pathogen *Streptococcus mutans*, influencing cell growth, death, interactions with other members of the oral flora and expression of known virulence traits. Bacteriocin production, biofilm formation, acid production and tolerance of acid and oxidative stresses by *S. mutans* all facilitate the competition, persistence and virulence of this organism in the human oral biofilm environment (Lemos and Burne, 2008). All of these traits are linked to the production of ComX (also called SigX), an alternative sigma factor that activates competence genes required for DNA uptake and processing. ComX production is controlled by a pathway that integrates signals received from two quorum sensing peptides (Shanker and Federle, 2016) with environmental cues such as pH (Guo *et al.*, 2014; Son *et al.*, 2015) and oxygen and reactive oxygen species (De Furio *et al.*, 2017), intracellular noise (stochasticity) and positive and negative feedback (Smith and Spatafora, 2012; Reck *et al.*, 2015; Leung *et al.*, 2015; Son *et al.*, 2015; Hagen and Son, 2017). As a result, *S. mutans* competence is a complex and heterogeneous behavior that can be exquisitely sensitive to the extracellular environment and that remains incompletely understood.

Population heterogeneity in *S. mutans* competence is evident from the low efficiency of natural genetic transformation (Li *et al.*, 2001), as well as from observations of cell-to-cell variability in *comX* gene expression (Lemme *et al.*, 2011; Son *et al.*, 2012; Reck *et al.*, 2015; Hagen and Son, 2017). Transformation efficiency in biofilms is typically less than 0.1% (Li *et al.*, 2001), while even under very favorable conditions no more than 10–50% of cells naturally express *comX* (Lemme *et al.*, 2011; Son *et al.*, 2012). In addition, the expression of *comX* can be bimodal or unimodal in the population, depending on the exogenous signals present, the growth phase and the environment (Son *et al.*, 2012; Shields and Burne, 2016). Post-translational regulation of ComX also appears to generate heterogeneity, as high levels of *comX* mRNA do

Accepted 21 May, 2018. *For correspondence. E-mail sjhagen@ufl.edu; Tel. 352 392 4716; Present addresses: †Physics Department, University of Florida, PO Box 118440, Gainesville FL 32611-8440.

not assure robust activation of *comY* (Seaton *et al.*, 2011). As with many other bacterial regulatory proteins (Inobe and Matouschek, 2008), ComX levels in *S. mutans* are modulated post-translationally by an ATP-dependent protease system composed of MecA and ClpCP (Tian *et al.*, 2013; Dong *et al.*, 2014; Dufour *et al.*, 2016). The MecA/ClpCP complex inhibits competence by targeting and degrading ComX, as it does in streptococci of the salivarius, mitis and pyogenic groups (Bjornstad and Havarstein, 2011; Boutry *et al.*, 2012; Wahl *et al.*, 2014; Li and Tian, 2017). However, the function of MecA/ClpCP within the *S. mutans* competence pathway, and particularly its role in cell-to-cell heterogeneity and the bimodal and unimodal competence behaviors, has not been explored in detail.

Fig. 1 summarizes the competence regulatory pathway in *S. mutans* (Smith and Spatafora, 2012; Tian *et al.*,

2013; Shanker and Federle, 2016). ComX activates late competence genes that include the nine-gene operon *comYA-I*, which contains seven genes that are required for transformation (Merritt *et al.*, 2005). Transcription of *comX* can be triggered by either of two quorum sensing peptides: CSP (competence stimulating peptide) or XIP (SigX-inducing peptide). The efficacy of these peptides is sensitive to environmental factors, including pH, oxidative stress, carbohydrate source and the peptide content of the medium (Son *et al.*, 2012; Son *et al.*, 2015; Moyer *et al.*, 2016; De Furio *et al.*, 2017).

CSP is derived from the ComC precursor, processed to a final length of 18 residues and exported to the extracellular medium. *S. mutans* detects CSP through the ComDE two-component signal transduction system (TCS), which directly activates multiple genes involved in bacteriocin

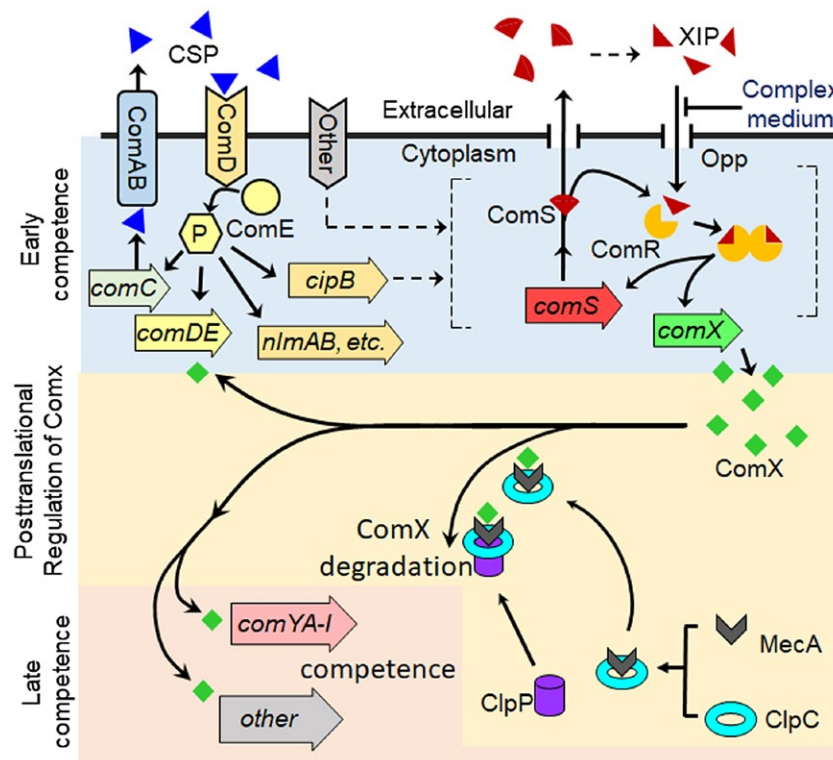


Fig. 1. *Streptococcus mutans* regulates genetic competence through multiple layers of control (Smith and Spatafora, 2012; Tian *et al.*, 2013; Shanker and Federle, 2016). Two quorum signals (CSP and XIP), together with other environmental inputs, drive the master competence regulator ComX, which is post-translationally regulated by the MecA/ClpCP proteolytic system. The peptide CSP (competence stimulating peptide) is detected by the ComDE two component system, leading to phosphorylation of the response regulator ComE, which activates transcription of bacteriocin genes such as *cipB*. Through a pathway not yet understood, activation of *cipB* is integrated with other environmental cues to stimulate the ComRS system, which is the immediate regulator of *comX*. ComX, also called SigX, is an alternative sigma factor that directly controls the nine-gene operon *comYA-I* and other genes required for transformation. The ComRS system includes the peptide ComS and the cytosolic receptor ComR. ComS is the precursor for the quorum-sensing peptide XIP (SigX-inducing peptide). In defined growth medium (lacking assorted small peptides), extracellular XIP is imported by the Ami/Opp permease and interacts with ComR to form a transcriptional activator for both *comS* and *comX*. As a result *comX* is uniformly (population-wide) activated in defined media containing XIP. In complex media, which are rich in assorted small peptides, extracellular XIP does not activate *comS* and *comX*; in this case XIP (or possibly its precursor ComS) is proposed to interact with ComR intracellularly, so that both *comS* and *comX* are driven by the bistable, intracellular transcriptional feedback loop involving *comS* and the ComRS complex (Son *et al.*, 2012). As a result *comX* is heterogeneously (bimodal in population) activated in complex media. The MecA/ClpCP system provides posttranslational regulation of ComX: The adapter protein MecA interacts with ClpC to target ComX for degradation by the protease ClpP. [Colour figure can be viewed at wileyonlinelibrary.com]

biogenesis, secretion and immunity. However, *S. mutans* ComDE does not directly activate *comX*. Instead, the ComRS system is the immediate regulator of *comX* in the mutans, salivarius, bovis and pyogenes groups of streptococci (Fontaine *et al.*, 2015). The ComRS system consists of the cytosolic receptor ComR and the 17 residue peptide ComS, which is processed by an unknown mechanism to form the 7 residue XIP (Mashburn-Warren *et al.*, 2010). Extracellular XIP is imported by the oligopeptide permease Opp and interacts with ComR to form a complex that activates the transcription of *comS* and *comX*. Exogenous XIP induces *comX* efficiently in chemically defined media lacking small peptides (such as FMC or CDM (Mashburn-Warren *et al.*, 2010; Son *et al.*, 2012)), leading to population-wide induction of *comX* at saturating XIP levels. However, XIP elicits no induction of *comX* in complex growth media containing small peptides, possibly owing to peptide competition with XIP for uptake by Opp. Interestingly, the CSP peptide signal has a different action than XIP, as it activates *S. mutans comX* only in complex growth media containing small peptides. It elicits no activity from *comX* in defined media that lacks small peptides, even though CSP stimulates the ComDE TCS (leading to bacteriocin production) under these conditions. In addition, the *comX* response to CSP is bimodal in the population, with no more than 50% of cells expressing *comX* at saturating CSP concentrations (Son *et al.*, 2012).

Consequently, the activation of *comX* in a population of *S. mutans* can exhibit two types of heterogeneity: a unimodal distribution when stimulated by exogenous XIP and a bimodal distribution when stimulated by exogenous CSP. Only the bimodal behavior requires an intact *comS*, whereas only the unimodal behavior requires the oligopeptide permease *opp*. We previously proposed that these different behaviors are two modes of operation of the transcriptional feedback loop associated with *comS*, which encodes its own inducing signal. In the unimodal case the cells import and respond to exogenous XIP, whereas in the bimodal case XIP import is blocked, leaving each cell to respond to its intracellular ComS (or XIP). The first mode allows a generally uniform, population-wide activation of *comX*, but the second mode leads to noisy, positive feedback dynamics in both *comS* and *comX* (Son *et al.*, 2012; Hagen and Son, 2017).

The mechanism of posttranslational control of ComX by MecA/ClpCP in *S. mutans* resembles that in pyogenic and salivarius streptococci, to which *S. mutans* MecA is closely homologous (Boutry *et al.*, 2012; Wahl *et al.*, 2014). *S. mutans* MecA is a 240 residue adapter protein that interacts with ComX and ClpC to form a ternary complex that sequesters ComX and targets it for

ATP-dependent degradation by the ClpP protease (Tian *et al.*, 2013; Dong *et al.*, 2014). MecA/ClpCP similarly controls the master competence regulators ComW in *S. pneumoniae* (Wahl *et al.*, 2014) and ComK in *Bacillus subtilis* (Turgay *et al.*, 1998). In *B. subtilis* MecA was shown to facilitate the ATP-dependent formation of the ClpCP proteolytic complex, which unfolds and degrades both MecA and its ComK target, and then itself dissociates (Turgay *et al.*, 1997; Turgay *et al.*, 1998; Kirstein *et al.*, 2006; Mei *et al.*, 2009; Wang *et al.*, 2011; Liu *et al.*, 2013). Therefore MecA/ClpCP operates dynamically by continuously turning over MecA as well as its regulatory target if present.

Several studies in *S. mutans* have established that MecA/ClpCP suppresses the activation of *comY* under CSP stimulation, in complex media (Tian *et al.*, 2013; Dong *et al.*, 2014; Dufour *et al.*, 2016). Deletion of *mecA*, *clpC* or *clpP* increased ComX levels and transformability during growth in complex media and also prolonged the competent state. These studies imply that MecA/ClpCP serves either to suppress *S. mutans* competence or to switch it off as growth progresses, in complex media. Some studies have found the puzzling result that deletion of *mecA* or *clpCP* caused a weaker increase in ComX levels or transformability – or even had no effect at all – in chemically defined media (with added XIP) than in complex media (with CSP) (Boutry *et al.*, 2012; Tian *et al.*, 2013; Dong *et al.*, 2014; Dufour *et al.*, 2016). A subsequent study found that MecA deletion improved *S. thermophilus* transformability in defined media, although the difference was attenuated at high levels of XIP stimulation (Wahl *et al.*, 2014).

The possible significance of growth media and the presence of heterogeneity raise the question of how MecA/ClpCP functions within the full competence pathway, in which the XIP and CSP signaling pathways activate *comX* in defined and complex media, respectively. Although it seems clear that MecA/ClpCP inhibits *comY* expression by sequestering and degrading ComX, a clearer model of how this regulation integrates with the known *comX* activation pathway, and how it may be overcome when competence is permitted, is still needed. Additional cell density signals (Dufour *et al.*, 2016), as well as XIP-dependent feedback or additional gene products (Wahl *et al.*, 2014), have been proposed as mechanisms for modulating ComX levels via MecA/ClpCP. We have used a single-cell, microfluidic approach to clarify some of these questions and to develop an explicit model of how MecA/ClpCP interacts with the noisy and bimodal mechanisms controlling *S. mutans comX*. Our data lead to a simple quantitative model that reproduces both the population average behavior and the cell-to-cell heterogeneity in *comY* activation.

Results

MecA/ClpCP affects XIP-induced transformation of *S. mutans*

The transformation efficiencies of the UA159 and *mecA/clpCP* deletion strains were measured for cells cultured in defined medium at various concentrations of synthetic XIP and are reported in Table 3 and in Supporting Fig. S1. Overall the deletion of *mecA*, *clpP* or *clpC* did not increase the transformation efficiency at the highest XIP concentrations. This finding is consistent with prior studies showing that deletions of *mecA/clpCP* do not necessarily enhance streptococcal transformability. Tian *et al.* (2013) and Dong *et al.* (2014) reported that the onset of XIP-induced transformability in *S. mutans* was slightly delayed by deletion of *mecA* and *clpC* although these deletions had little effect on the maximum transformation efficiency (Tian *et al.*, 2013; Dong *et al.*, 2014). Similarly in *S. thermophilus* the deletion of *clpC* (Bjornstad and Havarstein, 2011) or *mecA* (Boutry *et al.*, 2012) did not increase transformation efficiency in the presence of the ComS peptide. However our data show that XIP concentration modulates the effect of the *mecA* and *clpCP* deletions on *S. mutans* transformability. The transformation efficiencies of the *mecA* and *clpC* mutants begin at lower values in comparison to UA159 at low XIP concentrations, but dramatically increase as XIP is increased from 10 to 1000 nM XIP. This is evident in the fold change in transformability for *mecA* and *clpC* deletions in particular, as transformation of the *mecA* strain increased 100-fold and that of *clpC* increased 20-fold in this range of XIP concentrations. The effect of *clpP* is less pronounced, but still gives a higher fold change (~7 fold) over these XIP concentrations than does UA159 (~3-fold). Taken together these data support a role for the MecA/ClpCP system in the induction of *S. mutans* competence by XIP. To obtain more detailed insight into MecA/ClpCP and the control of *comY* under XIP stimulation we turned to individual cell studies.

Activation of *comX* leads to heterogeneous induction of *comY*

We used dual fluorescent reporters (*PcomX-gfp*, *PcomY-rfp*) to compare the activation of *PcomX* and *PcomY* in individual *S. mutans* supplied with exogenous XIP. Fig. 2A shows *S. mutans* UA159 growing in microfluidic channels under a constant flow of defined medium (FMC) that contains 0–2 μ M XIP. *PcomX* is activated in all cells if the XIP concentration exceeds about 100 nM, and its activation saturates as XIP exceeds about 800 nM. However, very few cells activate *PcomY* at XIP concentrations of 400 nM or less, and cells that do activate *PcomY* vary widely in their red fluorescence intensity. Even at 1–2 μ M XIP, many cells exhibit little *PcomY* activity.

Figures 2B and C show the statistical distribution of *PcomX* (GFP, upper rows) and *PcomY* (RFP, lower rows) reporter fluorescence for cells in response to exogenous XIP or CSP. Reporter fluorescence was imaged while cells grew in microfluidic channels under continuous flow of defined medium for XIP (Fig. 2B), or of complex medium for CSP (Fig. 2C). As previously reported (Son *et al.*, 2012), XIP in defined medium elicits a noisy but generally unimodal (population-wide) *comX* response. In contrast, CSP in complex medium elicits a much noisier, bimodal (double-peaked distribution) *comX* response. For both CSP and XIP stimulation, the response of *PcomY* is highly heterogeneous. Even the highest concentrations of CSP and XIP, which saturate the response of *PcomX*, incompletely activate *PcomY* in the population; the *PcomY* expression levels in individual cells span 2–3 orders of magnitude above the baseline. These data suggest that post-translational regulation of ComX increases cell-to-cell heterogeneity in *comY* expression, which adds to the noise in the *comX* response to CSP or XIP stimulation.

The MecA/ClpCP system inhibits the *comY* response to XIP and increases its noise

To test whether the MecA/ClpCP proteolytic system affects ComX function in defined medium, and to assess its effect on noise in *comY* expression, we compared *comX* and *comY* expression in dual reporter strains in the wild-type (UA159) and Δ *mecA* genetic backgrounds. Fig. 3 shows *PcomY* activity in individual cells that were stimulated by XIP in planktonic culture in defined medium and then imaged on glass slides. Similar results were obtained for cells growing in microfluidic flow channels. Deletion of *mecA* altered the *PcomY* response in two ways. First, the Δ *mecA* strain responded more strongly to XIP than did the wild-type. Unlike the wild-type genetic background, the Δ *mecA* cells showed high median *PcomY* expression, exceeding the baseline level at XIP concentrations greater than about 200 nM. Second, deletion of *mecA* reduced noise in *comY* expression (Fig. 3C and D). The difference in noise is apparent from the magnitude of the variability in the individual cell data, relative to the population median, which is indicated by the horizontal bars in Figs. 3A and C. The ratio of variability to median is clearly larger for UA159 than for Δ *mecA*. Therefore, although *comY* and *comX* expression correlated positively in UA159, the correlation was partially obscured by the noisy behavior of *comY*. In contrast, *comY* expression increased systematically as *comX* expression increased in the Δ *mecA* strain. Despite some noise in *comY*, a roughly proportional relationship can be discerned in the data of Fig. 3D,

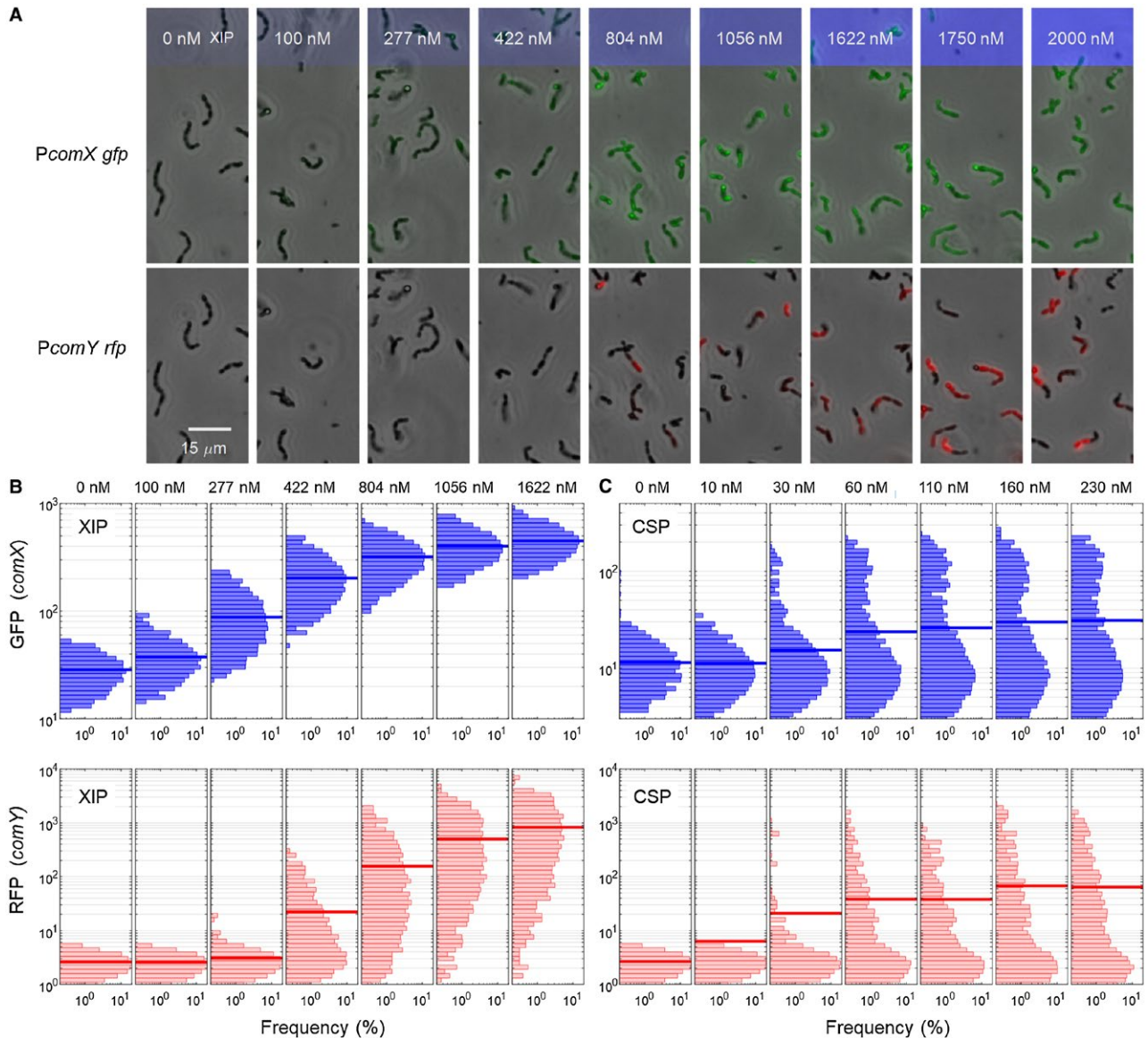


Fig. 2. (A) Microscopy images of dual reporter (*PcomX-gfp* and *PcomY-rfp*) UA159 *S. mutans* growing in microfluidic channels. Cells were supplied with the indicated concentrations of synthetic XIP by a continuous flow of defined medium. Phase contrast images (grayscale) are overlaid with fluorescence images showing *PcomX* (GFP, upper) and *PcomY* (RFP, lower) activity. (B)–(C) Histograms of *comX* (upper row) and *comY* (lower row) expression in dual reporter UA159 *S. mutans* under two different modes of stimulation. Cells growing in microfluidic channels were supplied with a continuous flow of (B) defined medium containing XIP, or (C) complex medium containing CSP, and were imaged in red (for *PcomY*) and green (for *PcomX*) fluorescence. XIP and CSP concentrations are indicated along the top of the figures. The length of each horizontal histogram bar indicates the percentage of cells that express at the level indicated. All axes are logarithmic. The thick blue or red bar in each histogram shows the population mean. [Colour figure can be viewed at wileyonlinelibrary.com]

but not in Fig. 3B. (The upward curvature in Fig. 3D results from the logarithmic horizontal axis.) The nearly linear correlation between *comY* and *comX* in the Δ *mecA* mutant suggests that, in the absence of MecA/CipCP, ComX activates *comY* in a direct and predictive fashion.

The effect of MecA on noise in *comY* is also seen in histograms of *comY* expression at given *comX* expression

levels. Supporting Fig. S2 shows *comY* histograms for cells growing in microfluidic channels with flowing defined medium and XIP, binned according to their *comX* activity. Both at high and low *comX* activity, the shape of the *comY* histograms is qualitatively different in the two strains. The deletion of *mecA* qualitatively alters the relationship between *comY* and *comX* expression in defined medium with addition of XIP.

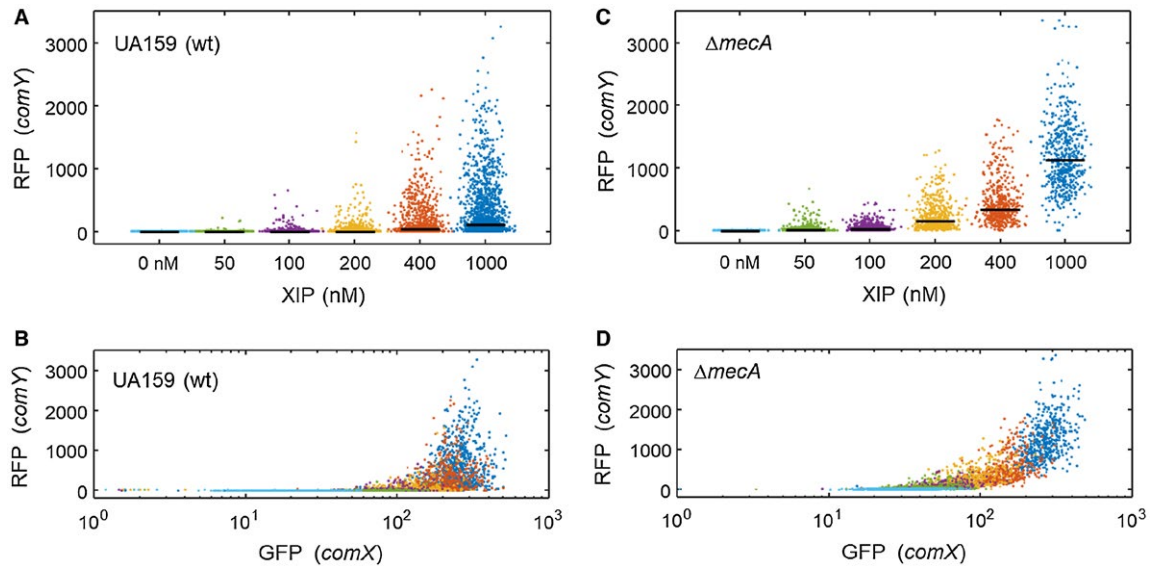


Fig. 3. Comparison of noise in *comY* activation by XIP in (A)-(B) UA159 (wild-type) and (C)-(D) $\Delta mecA$ deletion strain of *S. mutans*. Each point shows the RFP fluorescence of one cell that was incubated with XIP at the indicated concentration and then imaged on a glass slide. (A) and (C) show the dependence of *comY* expression on XIP stimulus in the two strains. The horizontal bar indicates the median expression. (B) and (D) show the correlation between *comY* and *comX* expression within individual cells, with the point colors indicating the XIP concentration in the same color code as (A) and (C). [Colour figure can be viewed at wileyonlinelibrary.com]

comY and *comX* expression are simply correlated in the absence of MecA

As is common for bacterial protein expression (Taniguchi *et al.*, 2010), the histograms of *PcomY* expression (Supporting Fig. S2) resemble a gamma distribution $\Gamma(nI, B)$, a two-parameter continuous probability distribution that can be interpreted in terms of sequential, stochastic processes of transcription and translation (see Experimental Procedures). This finding, together with the roughly linear correlation between *comY* and *comX* activity in the $\Delta mecA$ strain (Fig. 3D), motivates a simple mathematical model for *comX/comY* in the absence of MecA/ClpCP. The model is described in the *Experimental Procedures*: *comY* is activated in a mostly linear (but saturating) fashion by *comX* on average, but is also subject to stochasticity. The *comY* activity in a given cell is thus a random variable drawn from a gamma distribution whose parameters are determined by the *PcomX* activity in the cell. The model has four parameters, which we obtained through a maximum likelihood fit to the $\Delta mecA$ individual cell RFP and GFP fluorescence data of Fig. 3D. We then used these parameters to generate a stochastic simulation of the model for comparison to the data.

Fig. 4 compares the $\Delta mecA$ experimental data (Fig. 4A and B) with a simulation of the model (Fig. 4C and D). The model accurately reproduces both the population-averaged *comY* response and its cell-to-cell variability. This result indicates that in the absence of MecA/ClpCP regulation of ComX, *comY* can be modeled as a typical noisy

gene whose average activation is proportional to the concentration of active ComX protein.

A plausible alternative model is that extracellular XIP concentration, rather than *PcomX* activity *per se*, controls *comY* expression in $\Delta mecA$. The simulation shown in Supporting Fig. S3 indicates that the best fit of this model significantly overestimates the noise in *PcomY*. In short, modeling suggests that the *PcomX* activity of a $\Delta mecA$ cell is a straightforward predictor of its *PcomY* activity, and is also a better predictor than is the XIP concentration.

Different deletions in MecA/ClpCP produce different noise and threshold behaviors in comY

To determine which elements of the MecA/ClpCP system affect sensitivity and noise in *comY*, we measured *PcomY* and *PcomX* activity in the UA159, $\Delta mecA$, $\Delta clpC$ and $\Delta clpP$ genetic backgrounds (Fig. 5). All strains carried the dual fluorescent reporters and were imaged in microfluidic chambers while supplied with a continuous flow of defined medium containing XIP. In all strains, *PcomY* was more strongly activated at higher XIP concentrations where *PcomX* expression was higher, although noise and sensitivity varied among the different strains (Fig. 5A). All strains showed a similar dependence of *PcomX* activity (GFP) on XIP concentration (Fig. 5B). In the relation between *comY* and *comX* expression, the UA159 (wild-type) showed a more pronounced threshold in the onset of *comY* activation, at a *comX* level near 300 units, and

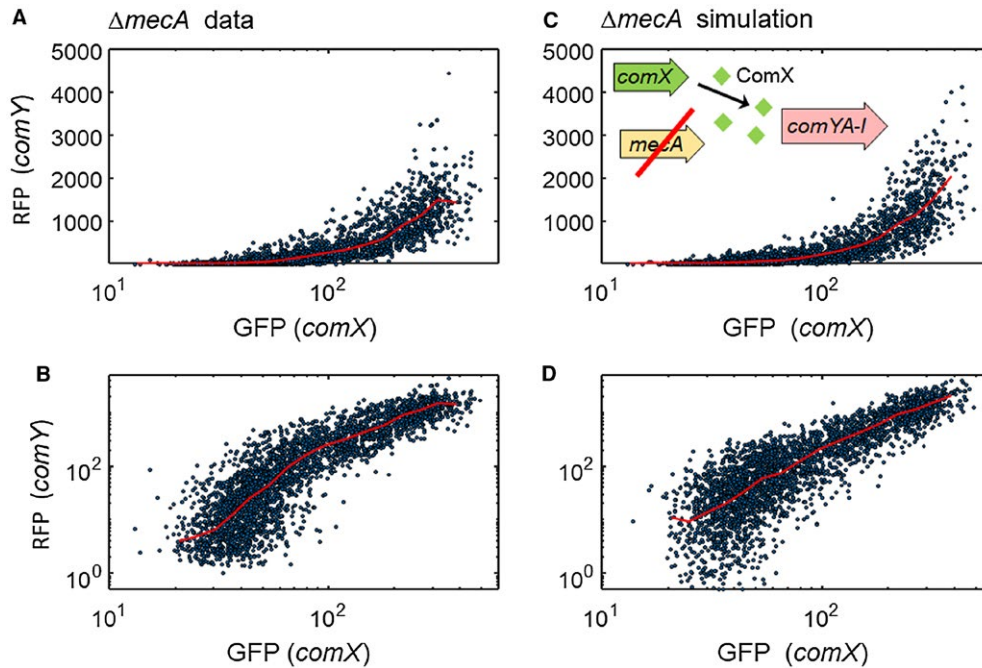


Fig. 4. Relation between P_{comY} and P_{comX} activity in the $\Delta mecA$ deletion strain, in response to XIP: (A)-(B) Experimental data of Fig. 3, showing correlation between P_{comX} and P_{comY} expression in $\Delta mecA$ cells subject to a range of XIP concentrations; (C)-(D) simulation of a stochastic model for $comX$ activation of $comY$. The stochastic model, described in *Experimental Procedures*, assumes that P_{comX} activity within each cell directly determines the probability distribution for P_{comY} activation in that cell. The upper and lower rows show the same data on linear and logarithmic vertical scales, respectively. The red curves show the median response. In (C)-(D) the GFP (horizontal) values are the same as in the experimental data of (A)-(B), while the RFP (vertical) values are generated from the stochastic model. Supporting Fig. S3 shows an additional comparison between the data and an alternative model in which the environmental XIP concentration, rather than P_{comX} activity, determines the probability distribution for P_{comY} activation. Model parameters are given in the legend to Supporting Fig. S3. [Colour figure can be viewed at wileyonlinelibrary.com]

much greater noise in $comY$ expression. The $clpP$ deletion strain, in which the MecA/ClpC complex can presumably bind, but not degrade, ComX, showed slightly less noisy $comY$ expression than the wild-type and $comY$ was somewhat more readily activated. Deletion of $clpC$, or especially $mecA$, reduced $comY$ noise significantly, such that the population was almost uniformly activated when P_{comX} expression was strong, near $1 \mu\text{M}$ XIP. Therefore, the interaction between MecA/ClpC and ComX, as well as the proteolytic action of ClpP on that complex, contribute to noise in $comY$ expression and also suppresses the ability of $comX$ expression to elicit the $comY$ response. Similar data were obtained when cells were grown in static medium and imaged while dispersed on glass slides.

The role of MecA alone can be modeled by simple sequestration of ComX

A detailed model for the regulation of ComX by MecA/ClpC must include the formation of the MecA/ClpC/ComX ternary complex, as well as the kinetics of ComX and MecA degradation by ClpP. Both of these mechanisms are absent in the $\Delta clpC$ strain, although the binary interaction of MecA with ComX is present. Therefore, we

tested whether a binary sequestration (MecA + ComX) model could reproduce our data for the activation of $comY$ by ComX in the $\Delta clpC$ strain. In this model, described in *Experimental Procedures*, individual ComX molecules are presumed to be tightly sequestered by individual MecA molecules, leaving them unavailable to stimulate $comY$ transcription. Then the probability distribution for the $comY$ expression of a cell becomes determined not by its $comX$ activity alone, but by the excess of ComX over MecA copy numbers. We modeled the MecA copy number as a random variable drawn from a gamma probability distribution; the activation of $comY$ by the available (unsequestered) ComX is modeled as in Fig. 4. The MecA probability distribution is presumed to be independent of XIP, consistent with our mRNA measurements showing no effect of XIP on $mecA$, $clpC$ or $clpP$ expression (Supporting Table ST1). Fitting this MecA model to the $\Delta clpC$ data therefore requires only a two-parameter fit for the gamma distribution parameters, which we obtained by maximum likelihood comparison of the data and model.

Fig. 6 compares the $\Delta clpC$ data with a stochastic simulation of this model. The $comY$ - $comX$ correlation closely resembles the experimental data, both in its average

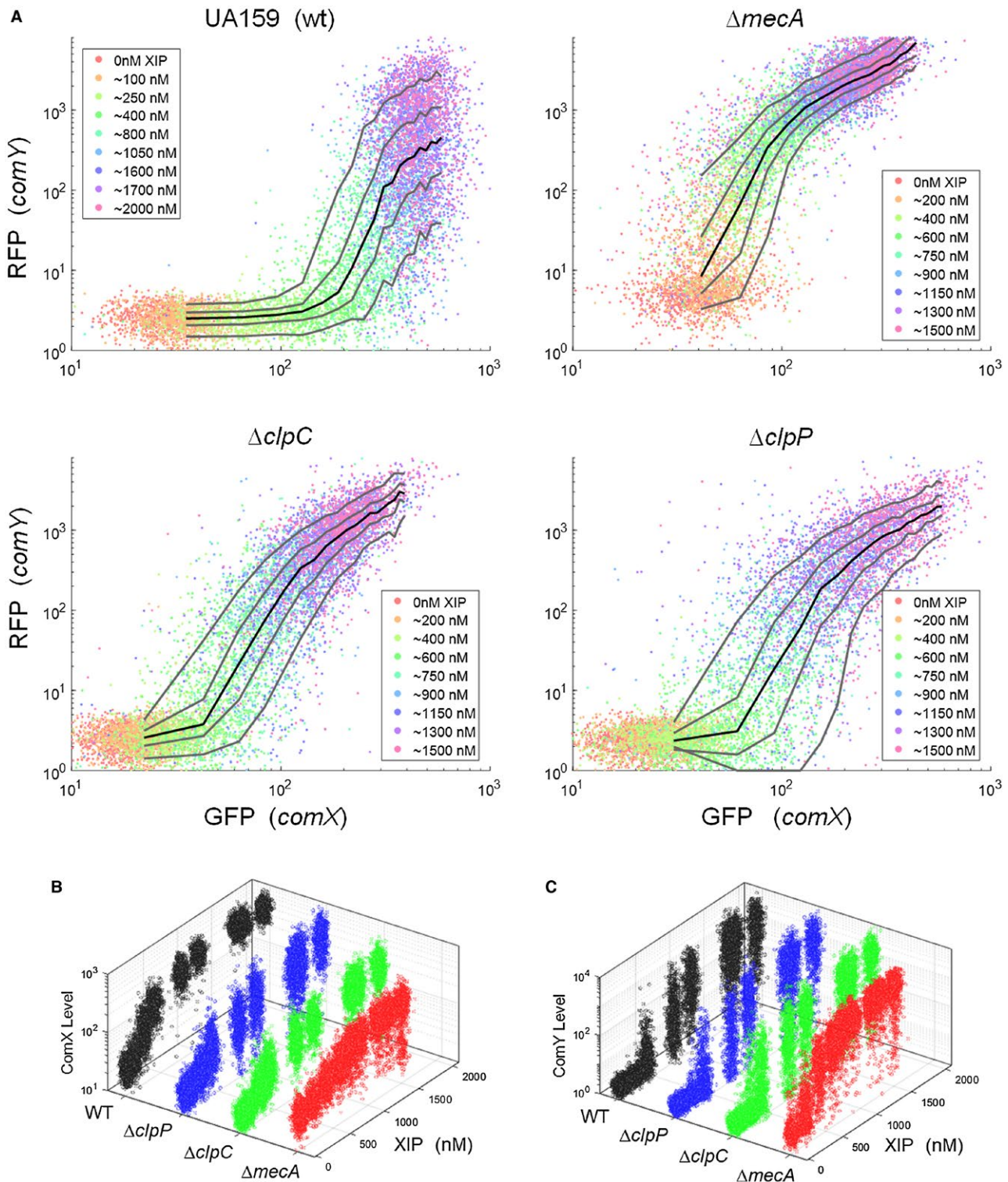


Fig. 5. A. Effect of *mecA/clpCP* deletions on the correlation between *comY* and *comX* activation. For each of the four strains (UA159, $\Delta mecA$, $\Delta clpP$, $\Delta clpC$) each point shows the P_{comY} and P_{comX} activity of one cell, as measured by RFP and GFP reporters, respectively. Cells were imaged while growing in microfluidic channels that were supplied with a continuous flow of defined medium that contained XIP concentrations as indicated by the point color. Approximately 1000 cells of each strain were imaged at each XIP concentration. Solid lines indicate the 10, 30, 50, 70 and 90th percentiles of P_{comY} activity. Cell autofluorescence contributes a background red fluorescence that is typically 1–5 fluorescence units in most experiments. Cell autofluorescence contributes a green background that is typically 20–30 fluorescence units. Supporting Fig. S6 shows the same data on linear axes.

B–C Scatterplots showing individual cell *comX* and *comY* expression versus exogenously added XIP in the four strains. [Colour figure can be viewed at wileyonlinelibrary.com]

trend and its noise. These results show that the higher *comY* expression noise that is observed in the $\Delta clpC$ strain, compared to the $\Delta mecA$ strain, is consistent with a mechanism where MecA suppresses *comY* response by sequestering ComX. Fitting the model to the data provides the probability distribution of the MecA copy number, Fig. 6C, where MecA is measured in units of equivalent *PcomX* activity. Cell-to-cell variability in MecA copy number is then a source of variability in *comY* expression.

CSP and XIP stimulation produce similar correlations between *comX* and *comY* activation

Previous studies have demonstrated that deletions of *mecA* or *clpCP* enhance *comY* expression upon stimulation with CSP in complex media (Tian *et al.*, 2013; Dong *et al.*, 2014). Our data show with single-cell resolution that the same deletions also affect the response to XIP in defined media. These findings raise the question of whether, in the presence of MecA/ClpCP, the activation of *comY* by ComX may be similar regardless of how *comX* transcription is induced, whether by XIP or CSP. Fig. 7 compares single-cell measurements of *comX* and *comY* activity with CSP and XIP, respectively. Precise quantitative comparison of the two response curves is complicated by the stronger green auto-fluorescence of cells in complex medium, which shifts the horizontal axis of the CSP data. Further, CSP appears to induce a slightly noisier *comY* response than does XIP, possibly in connection with feedback behavior in the ComDE system (Son *et al.*, 2015). However, the data verify a generally similar behavior in both conditions: *comY* responds in threshold fashion to activation of *comX*, and *comY* activation is highly heterogeneous in the population, even among cells with the highest *comX* activity.

Discussion

The MecA/ClpCP proteolytic system is well conserved as a negative regulator of genetic competence across streptococcal groups and in other naturally competent species, including *B. subtilis* (Liu *et al.*, 2013). However, while mechanistic studies of MecA/ClpCP have provided a clear description of its action, they have not fully resolved the question of how MecA/ClpCP contributes to competence regulation. Several authors have proposed that MecA/ClpCP serves either to suppress or terminate the competent state. For *B. subtilis*, Turgay *et al.* proposed that MecA/ClpCP degradation of the ComK competence regulator provides a 'timing' function by limiting synthesis

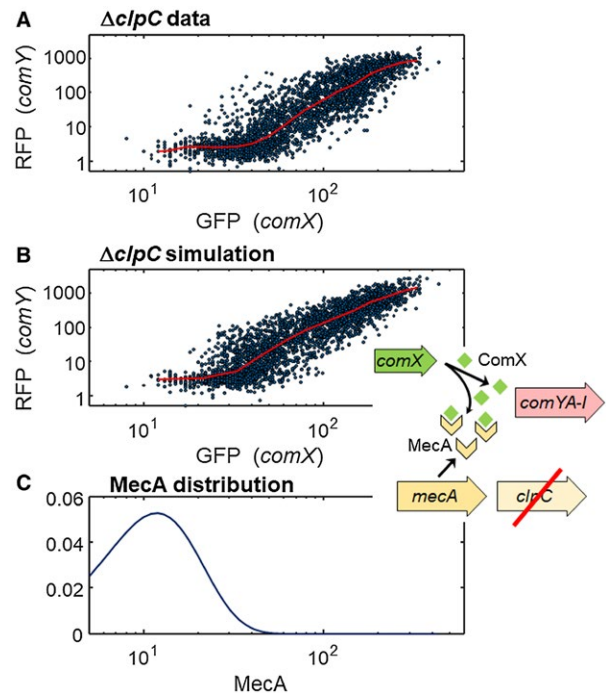


Fig. 6. Data and model for MecA sequestration of ComX.

A. Experimental measurement of *comX* activation of *comY* in dual-reporter (*PcomX-gfp*, *PcomY-rfp*) $\Delta clpC$ cells. Cells were provided 50–1000 nM XIP (defined medium) and then imaged on glass slides. The solid red line is the median *PcomY* response.

B. Simulation of a stochastic model (see Experimental Procedures) in which the activation of *PcomY* in each cell is determined by the excess of the cell's *PcomX* activity over its MecA level, where MecA levels obey a gamma statistical distribution. The simulation in (B) uses the MecA distribution (parameters $A = 3.61$, $B = 4.53$) that maximizes the likelihood of the data in (A). The baseline or background in *comY* is modeled by gaussian noise of 3 ± 0.8 red fluorescence units.

C. The statistical distribution of MecA levels used in generating the simulation of (B). MecA levels are referenced to *PcomX* expression levels: A MecA copy number of 10 implies MecA exactly sufficient to sequester all of the ComX produced when *PcomX-gfp* expression is at the level 10. [Colour figure can be viewed at wileyonlinelibrary.com]

of the auto-activating ComK regulator, thus permitting escape from the competent state (Turgay *et al.*, 1998). Dufour *et al.* proposed a similar model for *S. mutans*, in which the sequestration and degradation of free ComX by MecA/ClpCP forces an exit from the competent state late in growth, when the transcription of *comX* is repressed (Dufour *et al.*, 2016). Wahl *et al.* proposed that *S. thermophilus* MecA/ClpCP serves a 'locking' function, preventing the cell from entering the competent state under inappropriate conditions, such as early in the growth phase (Wahl *et al.*, 2014). Wahl *et al.* argued that at low XIP concentrations proteolytic degradation of ComX prevents competence, but that high XIP concentrations may alleviate this repression, possibly by overwhelming the proteolytic capacity or by activating another, unidentified gene product.

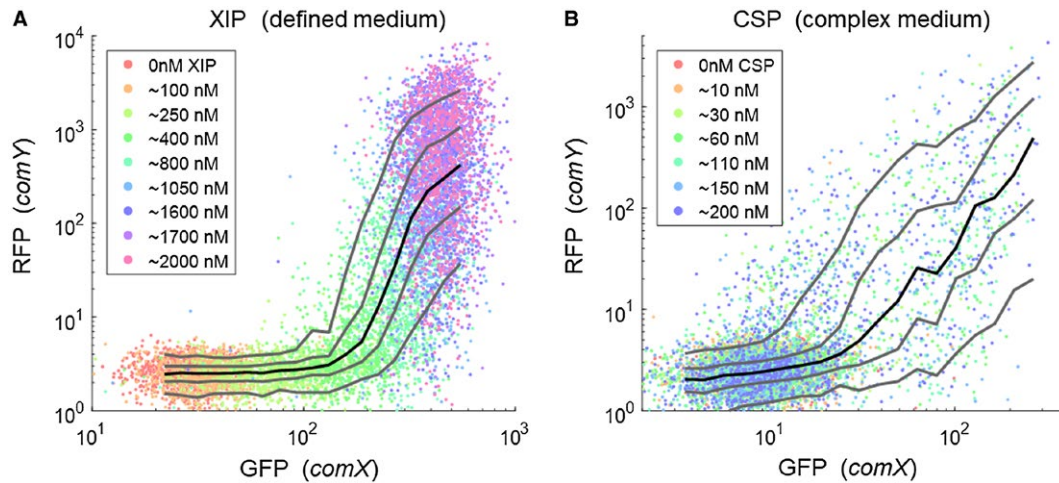


Fig. 7. Comparison of *comX/comY* correlation in UA159 background in response to XIP and CSP. Cells were imaged while adhered in microfluidic flow channels supplied with continuous flow of (A) defined medium containing XIP or (B) complex medium containing CSP. Solid lines indicate the 10, 30, 50, 70 and 90th percentiles of *PcomY* activity. Horizontal scales are not strictly equivalent owing to higher autofluorescence baseline of cells in the complex media. [Colour figure can be viewed at wileyonlinelibrary.com]

Both the ‘locking’ and ‘timing’ models interpret MecA/ClpCP as a mechanism for suppressing activation of *comY* when *comX* expression is weak. Our data are consistent with this description. Moreover, our data show that this suppression can be described by the simplest model in which an intracellular pool of MecA intercepts available ComX, sequestering it and blocking its otherwise straightforward activation of *comY*. Such a model quantitatively fits the data on the *clpC* mutant, in which MecA can sequester ComX but *clpP* proteolysis is absent. If the MecA copy number obeys a gamma probability distribution, as is common for bacterial proteins, then the model reproduces both the average relationship between *comY* and *comX* expression and the cell-to-cell variability in that expression. Therefore, the response of *comY* in individual *clpC* and *mecA* cells can be understood solely in terms of the *PcomX* activity and MecA copy number distribution. The behavior of the late competence genes in these mutants can be understood without positing any role for XIP other than as a stimulus for *PcomX*.

In addition, our single-cell data show that the MecA/ClpCP system substantially enhances the noise (cell-to-cell heterogeneity) in *comY* expression when *comX* is activated. Even at high XIP concentrations that saturate *comX* expression, *comY* expression levels within the UA159 population span a range extending three orders of magnitude above the baseline; by contrast, the deletion mutants all express *comY* with far less noise at high XIP concentrations. Our modeling indicates that cell-to-cell variability in the MecA copy number in wild-type cells, together with the proteolytic action of ClpP (which reduces MecA and ComX copy numbers) adds to noise that is generated upstream by the pathways that activate

comX. The resulting noisy threshold effect is very similar to the toxin/antitoxin competition that generates phenotypic heterogeneity in bacterial persistence (Rotem *et al.*, 2010), or to a sequestration-induced threshold model for nonlinear gene regulation (Buchler and Cross, 2009).

A clear understanding of the role of MecA/ClpCP has perhaps been complicated by early reports that deletion of *mecA* or *clpC* increased transformability or ComX protein levels under CSP stimulation (in complex medium), but not under XIP stimulation (in defined medium). Our data confirm in detail that the MecA/ClpCP system affects signaling from *comX* to *comY* in defined medium. In fact, as the sequestration model described above is indifferent to whether *comX* is stimulated by exogenous XIP or CSP, we expect that signaling from *comX* to *comY* should be similar in both CSP/complex medium and in XIP/defined medium. Fig. 7 suggests that the relationship is very similar.

This finding suggests that the MecA/ClpCP system acts continuously to suppress ComX levels, regardless of the extracellular inputs driving *comX* expression. A model where MecA/ClpCP performs this task in relatively steady fashion is consistent with findings that *S. mutans* MecA and ClpCP protein levels did not differ in complex and defined medium (Dong *et al.*, 2014), that MecA induction showed little change during *S. suis* competence (Zaccaria *et al.*, 2016), and that *S. mutans mecA/clpCP* mRNA levels are insensitive to XIP inputs (Supporting Table ST1). Thus competence will be suppressed when *comX* is weakly expressed due to insufficient CSP or XIP early in growth (‘locking’ behavior). Competence will also be suppressed when *comX* is weakly expressed late in growth due to inefficient CSP/XIP signaling. Falling extracellular

pH late in the growth phase suppresses competence signaling by CSP and XIP (Guo *et al.*, 2014; Son *et al.*, 2015), which may allow MecA/ClpCP to shut down the competent state ('timing behavior').

Consequently the sequestration mechanism can provide both 'timing' and 'locking' functions.

The simulations in Fig. 4 and Fig. 6 are based on simple equilibrium models that address only the effects of sequestration by MecA on the pool of free ComX, omitting the kinetic effects of ClpCP unfolding and degradation of ComX and MecA. A model that includes ClpP proteolysis is much more complicated, as it must include the sequential binding steps that are associated with the formation of the ternary complex, binding of ClpP, and the breakdown of both MecA and ComX. The binding and kinetic parameters of the model cannot be determined from our data; however we can construct a reasonably tractable model for the full system by simplifying the complex regulatory mechanism that is outlined in the literature (Mei *et al.*, 2009). Supporting Fig. S7 describes a simplified kinetic model that can rationalize some of the observations in our data, including the finding that deletion of *clpC* or *clpP* did not eliminate the *comX* threshold that is required for *comY* activation, and that only the *mecA* deletion eliminated the threshold and sharply reduced the noise in *comY*. Supporting Fig. S7 shows that simulations from such rough models can reproduce key differences in *comX-comY* threshold behavior observed among the mutants studied here.

We note that a MecA copy number distribution that has higher mean but is narrower than that of Fig. 6C would still provide the same 'timing' or 'locking' function without introducing as much noise in *comY*. The evident width of the distribution therefore suggests that the organism may benefit from greater noise. The competence pathway in *S. mutans* is linked to several stress-induced behaviors that are heterogeneous in the population, including competence, lysis and a persister phenotype (Perry *et al.*, 2009; Leung *et al.*, 2015; Leung *et al.*, 2015). A link between quorum controlled behavior and phenotypic heterogeneity has often been noted in bacterial gene regulation. In other organisms, such as *B. subtilis*, complex pathways that integrate intracellular and extracellular signaling mechanisms with stochastic gene expression often generate phenotypic heterogeneity, distributing stress response behaviors such as competence and sporulation among different individuals in the population (Smits *et al.*, 2006; Dubnau and Losick, 2006; Veening *et al.*, 2008; Grote *et al.*, 2015). Interestingly, propidium iodide staining of individual *S. mutans* indicates that *comX*-driven lysis is decoupled from *comX*-driven competence (Supporting Fig. S5). While higher *comX* expression increases the probability of cell lysis, the most highly expressing cells (which are more likely to express *comY*) actually show

less evidence of lysis. Accordingly, the MecA/ClpCP system may provide a bet-hedging advantage to an *S. mutans* population by providing an additional, stochastic switching point in the regulatory pathway from stress conditions to transformability.

Our data show that the action of the *S. mutans* MecA/ClpCP system can be quantitatively understood, at the level of individual cell behavior, within a very simple threshold mechanism. As the MecA/ClpCP system is widely conserved this finding raises the question of whether MecA/ClpCP also generates a heterogeneity advantage in other organisms such as *S. pneumoniae*, in which competence regulation is more straightforward and the *comX* bimodality mechanism is absent. Our data also highlight the long-standing question of whether by combining cooperative behaviors of quorum signaling with deliberately noisy intracellular phenomena such as MecA and ComRS, *S. mutans* can achieve some form of optimum balance between socially driven, environmentally driven and purely stochastic behavior in competence regulation.

Experimental procedures

Preparation of reporter strains

S. mutans strains and deletion mutants (Table 1) harboring green fluorescent protein (*gfp*) and/or red fluorescent protein (*rfp*) reporter genes fused to the promoter regions of *comX* (*PcomX-gfp*) and *comY* (*PcomYA-rfp*) were grown in brain heart infusion medium (BHI; Difco) at 37°C in a 5% CO₂, aerobic atmosphere with either spectinomycin (1 mg mL⁻¹), erythromycin (10 µg mL⁻¹) or kanamycin (1 mg mL⁻¹). *PcomX-gfp* was directly integrated into the chromosome of *S. mutans* (denoted XG) by amplifying a 0.2 kbp region comprising *PcomX* using primers that incorporated *Xba*I and *Spe*I sites (Table 2). This was fused to a *gfp* gene that had been amplified with primers engineered to contain *Spe*I and *Xba*I sites from the plasmid pCM11 (Lauderdale *et al.*, 2010; Son *et al.*, 2012), and inserted into the *Xba*I site on pBGE (Zeng and Burne, 2009). *PcomYA-rfp* was constructed in shuttle vector pDL278 (LeBlanc *et al.*, 1992) by amplification of a 0.2 kbp region containing *PcomY* with *Hind*III and *Spe*I site-containing primers and fusing with the DsRed.T3(DNT) *rfp* gene reporter fragment amplified from plasmid pRFP (Bose *et al.*, 2013), using primers that incorporated *Spe*I and *Eco*RI sites. The ligation mixtures were transformed into competent *S. mutans* (strain designated YR) and into the XG strain (denoted XG&YR). Additionally, to study the role of MecA/ClpCP on *PcomY* expression, both the XG integration vector and the YR shuttle vector were transformed into strains harboring non-polar (NPKmR) antibiotic resistance cassette

replacements of *mecA* (this study), *clpC* or *clpP* (Lemos and Burne, 2002). Plasmid DNA was isolated from *Escherichia coli* using a QIAGEN (Chatsworth, Calif.) Plasmid Miniprep Kit. Restriction and DNA-modifying enzymes were obtained from Invitrogen (Gaithersburg, Md.) or New England Biolabs (Beverly, Mass.). PCRs were carried out with 100 ng of chromosomal DNA using Taq DNA polymerase. PCR products were purified with the QIAquick kit (QIAGEN). DNA was introduced into *S. mutans* by natural transformation and into *E. coli* by the calcium chloride method (Cosloy and Oishi, 1973).

Competence peptides

Synthetic CSP (sCSP, sequence = SGSLSTFFRLFNRS-FTQA), corresponding to the mature 18 residue peptide (Hossain and Biswas, 2012) was synthesized by the Interdisciplinary Center for Biotechnology Research (ICBR) facility at the University of Florida and its purity (95%) was confirmed by high-performance liquid chromatography (HPLC). The CSP was reconstituted in water to a final concentration of 2 mM and stored in 100 μ L aliquots at -20°C . Synthetic XIP (sXIP, sequence GLDWWSL), corresponding to residues 11–17 of ComS, was synthesized and purified to 96% homogeneity by NeoBioSci (Cambridge, MA). The lyophilized XIP was reconstituted with 99.7% dimethyl sulfoxide (DMSO) to a final concentration of 2 mM and stored in 100 μ L aliquots at -20°C .

Microfluidic mixer design and fabrication

Microfluidic devices were fabricated by the soft lithography method of molding a transparent silicon elastomer (polydimethylsiloxane) on a silicon master (Sia and Whitesides, 2003). The master was made from a silicon

wafer through conventional photolithographic processing. Details of the fabrication method and the devices were described previously (Jeon *et al.*, 2000; Son *et al.*, 2012; Son *et al.*, 2015). Briefly, the microfluidic device consisted of nine parallel flow chambers (each 15 μ m deep and 400 μ m wide). Three inlet channels supplied media containing different concentrations of signal peptides, delivered by syringe pumps into the device. The design has a mixing network that generates nine streams containing different admixtures of the three input solutions. These streams flow through the nine cell chambers in which *S. mutans* are adhered to the lower, glass window. The device also has two side channels: one for the control of fluid inside the device and the other for injection of different solutions into the cell chambers. Two-layer lithography allows air pressure control of these side channels during cell loading and injection of different solutions (Unger *et al.*, 2000).

Microfluidic experiments

Overnight cultures grown in BHI with antibiotic selection were washed and diluted 20-fold in fresh medium, which was either chemically defined medium (FMC) (Terleckyj *et al.*, 1975; De Furio *et al.*, 2017) or a complex medium that consisted of 1/3 of BHI (BD) and 2/3 of FMC by volume. Cultures were then incubated at 37°C in a 5% CO_2 , aerobic atmosphere. When OD_{600} reached 0.1–0.2, cells were sonicated at 30% amplitude for 10 s (Fisher FB120) to separate cell chains and then loaded into the microfluidic device. Each cell chamber was continuously perfused with fresh medium containing different amounts of synthetic XIP (0–2 μM) or synthetic CSP (0–1 μM). The XIP or CSP concentration in each flow channel was generated by the mixture of three different inlet media in the mixing network in the device. A trace amount (0–10 ng/mL) of far-red fluorescent dye (Alexa Fluor 647) was added to each of the three inlet media in proportion to its signal molecule concentration, so that the concentration of signal molecule in each chamber could be calculated. After 2.5 hr of incubation time, fresh medium containing 100 $\mu\text{g mL}^{-1}$ of rifampicin was flowed through all cell chambers to halt GFP and RFP transcription. Cell chambers were then incubated an additional 3 hr to allow the full maturation of RFP. Cells were imaged in phase contrast and in green and red fluorescence using an inverted microscope (Nikon TE2000U) equipped with a computer controlled motorized stage and cooled CCD camera. Approximately 700 to 1000 cells were studied for each condition shown in the histograms. The microfluidic study of *comY* and *comX* response to XIP in the mutant strains was repeated three times. The same experiment was also performed on cells that were dispersed on

Table 1. Strains used in this study. Em^r, erythromycin; NPKm^r, non-polar kanamycin; Sp^r, spectinomycin.

<i>S. mutans</i> strains	Characteristic(s)	Source
WT (UA159)	<i>S. mutans</i> wild-type strain	ATCC 700610
XG	P _{comX} - <i>gfp</i> integrated into UA159, Em ^r	This study
YR	UA159 harboring P _{comY} - <i>rfp</i> , Em ^r	This study
XG&YR	XG harboring P _{comY} - <i>rfp</i> , Sp ^r	This study
XG&YR& Δ <i>mecA</i>	Δ <i>mecA</i> ::NPKm ^r into XG&YR	This study
XG&YR& Δ <i>clpC</i>	Δ <i>clpC</i> ::NPKm ^r into XG&YR	This study
XG&YR& Δ <i>clpP</i>	Δ <i>clpP</i> ::NPKm ^r into XG&YR	This study

Table 2. Primers used in this study. Underline of nucleotide sequence denotes respective restriction enzyme site.

Primer	Nucleotide Sequence (5' – 3')
<i>PcomX</i> -XbaI-FW	GGA TCT AGA CCA ATT TCA AAT AAT G
<i>PcomX</i> -SpeI-RV	CTT <u>CAC TAG</u> TCT ATT ACG ATG ACC
<i>PcomY</i> -HindIII-FW	ACA <u>AAG CTT</u> AAA CAA AAT GAT ACC C
<i>PcomY</i> -SpeI-RV	TCG <u>ACT AGT</u> CCA GGA AAA AAT TAG
<i>rfp</i> -SpeI-FW	GAC <u>TAG TTG</u> ATT AAC TTT ATA AGG AGG AAA AAC ATA TGG A
<i>rfp</i> -EcoRI-RV	CGG AAT TCT TAT AAA AAC AAA TGA TGA CGA CCT TCT GTA C
Δ <i>mecA</i> -FW	GAT <u>GAC TGG</u> CTG GAT GCA CA
Δ <i>mecA</i> -BamHI-FW	TTT <u>GGA TCC</u> CAT AGT CTT TAC CTC A
Δ <i>mecA</i> -BamHI-RV	ATG <u>GGA TCC</u> TAA GCT AGA TGA TAC C
Δ <i>mecA</i> -RV	CCA AAC CAT CCA AAC CAT CAA

Table 3. Transformation efficiencies measured in defined medium.

Synthetic XIP (nM)	UA159	Δ <i>mecA</i>	Δ <i>clpC</i>	Δ <i>clpP</i>
10	3.26 ± 0.99 e-5	6.23 ± 2.01 e-7	5.30 ± 2.74 e-7	6.31 ± 1.45 e-6
25	5.24 ± 1.40 e-5	1.35 ± 0.54 e-5	1.15 ± 0.37 e-6	8.47 ± 2.22 e-6
50	5.95 ± 2.34 e-5	3.14 ± 0.84 e-5	2.04 ± 0.85 e-6	8.81 ± 1.97 e-6
75	4.85 ± 0.98 e-5	4.21 ± 1.40 e-5	2.43 ± 0.73 e-6	9.21 ± 2.73 e-6
100	5.51 ± 3.59 e-5	7.92 ± 1.08 e-5	5.49 ± 1.32 e-6	1.86 ± 0.78 e-5
300	9.07 ± 3.11 e-5	1.02 ± 0.42 e-4	1.11 ± 0.20 e-5	3.57 ± 1.03 e-5
1000	9.65 ± 2.59 e-5	5.78 ± 0.55 e-5	1.19 ± 0.20 e-5	4.34 ± 2.91 e-5

glass slides, giving closely similar results. Similarly the microfluidic study of *comY* and *comX* response to CSP stimulation in UA159 was repeated three times.

Single cell image analysis

Custom Matlab software was used to analyze the expression of the *gfp* and *rfp* reporters in individual cells from overlaid phase contrast, GFP and RFP images (Kwak *et al.*, 2012). The software first segments individual cells from the cell chain based on the phase contrast image, then finds the concentration of GFP and RFP by correlating the intensity of the phase contrast image with its GFP and RFP fluorescence intensity. This gives a unitless parameter (denoted *R*) that is proportional to the intracellular concentration of GFP or RFP. The GFP or RFP expression levels shown in the data figures are the *R*-values for green or red cell fluorescence respectively.

Transformation efficiency

Overnight cultures of selected strains were grown overnight in BHI medium with appropriate antibiotic ($n = 8$ replicates). The next day, cultures were diluted 1:20 in 200 μ L of FMC medium in polystyrene microtiter plates and grown to $OD_{600} = 0.15$ in a 5% CO_2 atmosphere. At this time, different synthetic XIP concentrations (10–1000 nM) and 0.5 μ g of purified plasmid pIB184, which harbors

a erythromycin resistance (ErmR) gene, were added to the cultures. After 2.5 hr incubation at 37°C, transformants and total CFU were enumerated by plating appropriate dilutions on BHI agar plates with and without the addition of 1 mg mL⁻¹ erythromycin, respectively. CFU were counted after 48 hr of incubation, and transformation efficiency was expressed as the percentage of transformants among the total viable cells.

RFP expression and stability

To verify that the codon-optimized variant of DsRed.T3 *rfp* reporter produces similar results to *gfp*, UA159 harboring *PcomX-rfp* plasmid was grown in a static BHI or FMC medium. When the OD_{600} reached ~0.2, each culture was divided into two samples, with and without the signaling peptide, respectively. 1 μ M synthetic CSP was the signal for the BHI sample and 500 nM synthetic XIP was the signal for the FMC sample. After 2 hours of stimulation, rifampicin was added. Samples were incubated an additional 3 hr for RFP maturation, and their RFP expression was measured. Supporting Fig. S4A shows that the RFP fluorescence successfully captured the distinct bimodal (CSP) and unimodal (XIP) response of *comX* under these conditions.

To test the maturation time of the RFP protein (Supporting Fig. S4B), UA159 harboring *PcomX-gfp* and *PcomY-rfp* was grown in static FMC medium. When the

OD₆₀₀ reached ~ 0.2, 2 μM synthetic XIP was added to induce RFP production. After additional incubation of 2 hr, 100 μg/mL of rifampicin was added. Then RFP fluorescence was measured every hour up to 5 hr. Supporting Fig. S4B shows that fluorescence saturated between 2 and 3 hr, suggesting 3 hr is sufficient waiting time for RFP maturation. The corresponding half-time of ~1.4 hr is in good agreement with the reported DsRed. T3 maturation half time of ~1.3 at 37 °C (Bevis and Glick, 2002).

To test the expression and stability of the RFP protein (Supporting Fig. S4C and S4D) in the different mutant backgrounds used in this study, the RFP gene was transcriptionally linked to the constitutive promoter (Pveg) (Radeck *et al.*, 2013) by cloning into HindIII and SpeI sites on the pDL278 plasmid. Following ligation, the selected construct was then transformed into each of the UA159, Δ*mecA*, Δ*clpP* and Δ*clpC* backgrounds with colonies selected by spectinomycin resistance and confirmed by sequencing. After a 1:25 dilution from overnight cultures, cells were grown to late mid-exponential growth phase (OD₆₀₀ nm = 0.8) in BHI medium. A final concentration of 35 μg/mL chloramphenicol was then added to the cultures to halt protein translation (*t* = 0 hr). A fraction of the culture was harvested at selected time points after chloramphenicol addition (0, 1, 3 and 6 hr). Whole cell lysates from each fraction were obtained by mechanical disruption (bead beating) and 10 μg was loaded and run on a 4–20% gradient Mini-PROTEAN TGX gel (BioRad). Following transfer to a polyvinylidene difluoride (PVDF) membrane (BioRad), the RFP protein was probed for with a Living Colors DsRed Polyclonal Antibody (Takara Bio USA, Inc) according to the supplier's protocol.

For the single-cell fluorescence measurements of Supporting Fig. S4D, cultures of the deletion and wild-type strains were grown in BHI overnight with 1 mg/mL spectinomycin. Cultures were then washed twice in FMC, diluted 20-fold and ultrasonicated before being resuspended in FMC. Cultures were then incubated at 37°C to OD₆₀₀ ≈ 0.1. Aliquots were then removed at hourly intervals, dispersed on glass slides, and the cells imaged in phase contrast and fluorescence. Fluorescence data shown were collected at 3 hr.

mRNA levels for *mecA*, *clpCP* and *com* genes

Data for the analysis of relative mRNA levels for *mecA*, *clpCP* and *com* genes are from RNA-Seq analysis completed on strain UA159 (Kaspar *et al.*, 2018, in preparation). The wild-type strain was grown in FMC medium to OD₆₀₀ = 0.2, at which time either a final concentration of 2 M XIP or vehicle control (1% DMSO) was added. The strains were then allowed to grow to mid-exponential

phase (OD₆₀₀ = 0.5) before harvesting. From the analyzed RNA-Seq data, total read counts for each selected gene were found from three biological replicates and RPKM (reads per kilobase per million) calculated under each condition. Finally, ratios for mRNA levels were found using the normalized RPKM data and by setting *mecA* levels to 1.0. The data files used in this study are available from NCBI-GEO (Gene Expression Omnibus) under accession no. GSE110167.

Stochastic model for MecA regulation of *comX*

We used the gamma statistical distribution to model cell-to-cell variability (noise) in the activation of *comY* by ComX and the effect of the MecA/ClpCP system. Heterogeneity in bacterial protein copy number can be well described by a physical model of transcription and translation as consecutive stochastic (Poisson) processes, characterized by rates k_r (transcripts per unit time) and k_p (protein copies per transcript per unit time), respectively (Friedman *et al.*, 2006; Taniguchi *et al.*, 2010). In this model, the protein copy number n in each cell is a random variable drawn from a gamma distribution $\Gamma(n | A, B)$. The two parameters A and B that determine the shape of the distribution are related to k_r and k_p , respectively (and to the mRNA and protein lifetimes) (Friedman *et al.*, 2006). Gamma distribution fits to our *PcomY* reporter data are shown in Supporting Fig. S2.

To model ComX activation of *comY* in the *mecA* deletion mutant (lacking post-translational regulation by MecA/ClpCP), we applied a simple quantitative model in which the *PcomX* activity of each cell, as reported by GFP fluorescence, determines the gamma distribution for its *PcomY* activity, measured by RFP fluorescence. Specifically, the *PcomY-rfp* reporter fluorescence Y of a cell is a random number drawn from a gamma distribution $\Gamma(Y | A, B)$, for which the parameters are

$$A = a_1 X / (X + a_2)$$

$$B = b_1 X / (X + b_2)$$

Here, X is the *PcomX-gfp* reporter fluorescence of that cell. Thus Y is directly activated by X in a saturating but noisy fashion. We fit this model to a dataset of individual cell RFP and GFP fluorescence values collected on dual reporter (*PcomX-gfp*, *PcomY-rfp*) Δ*mecA* cells that were supplied with different concentrations of synthetic XIP (defined medium) and then imaged on glass slides. Maximum likelihood analysis gives the four model parameters a_1 , a_2 , b_1 , b_2 for the Δ*mecA* strain as follows: we start with the experimental *PcomX* activity measured for each cell, then use the four parameters to define a *PcomY* gamma distribution for that cell. We find the probability of

that cell's actual *PcomY* activity, given that gamma distribution. The parameter values are then adjusted to maximize the likelihood of the total dataset. (The optimal values are given in Supporting Fig. S3.) Given these model parameters we then generate a model simulation for comparison against the data as follows: we use the model parameters and the measured *PcomX* activity of each cell to generate its *PcomY* gamma distribution, draw a random number from that distribution to obtain a simulated *PcomY* activity for the cell, and then plot the resulting simulated *PcomY* vs *PcomX* values for all cells (Fig. 4C, 4D).

We also tested an alternative model in which environmental XIP concentration, rather than *PcomX* activity of a cell, is the determinant of that cell's *PcomY* activity. In this model, *X* in the above equations refers to the XIP concentration supplied to a cell. Again, using maximum likelihood, we found the parameters (a_1 , a_2 , b_1 , b_2) that gave best agreement with the $\Delta mecA$ data in this alternative model. The scatterplot of Supporting Fig. S3C, generated by the above simulation procedure, compares the simulated *PcomY* to the experimental *PcomY* for the $\Delta mecA$ data.

For the dual-reporter $\Delta clpC$ mutant, we extended the above model by allowing *MecA* to sequester, but not degrade *ComX*. For simplicity, we assume that (i) *MecA* and *ComX* bind with sufficiently high affinity that a cell can only activate *comY* to the extent that its *ComX* copy number exceeds its number of *MecA* copies, leaving some available *ComX*; (ii) The activation of *comY* by the available *ComX* is as described in the $\Delta mecA$ model above (and with the same parameters); (iii) the *MecA* copy number M in a cell is a stochastic variable drawn from a gamma distribution $\Gamma(M | A, B)$ whose A and B parameters are fixed, independent of XIP concentration. If X is the *PcomX-gfp* activity of a given cell, then $X' = X - M$ is the amount of *ComX* available after sequestration by *MecA*. Given a GFP measurement of X for a cell, the *MecA* gamma distribution $\Gamma(M = X - X' | A, B)$ determines the probability that X' copies of *ComX* are available to activate *comY*. This X' determines the probability distribution for Y (the *PcomY-rfp* response) by the above model. Averaging over the *MecA* distribution then gives a prediction for both the average behavior and cell-to-cell variability in the dependence of *PcomY-rfp* on *PcomX-gfp*, in the presence of *MecA*.

Taking the *PcomY-rfp* activation parameters obtained in the $\Delta mecA$ fit, we therefore analyzed individual cell *PcomX/PcomY* data that was collected on $\Delta clpC$ cells that were supplied with different XIP concentrations and imaged on glass slides. We then found the A and B values for the *MecA* distribution that maximize the likelihood of the *PcomX/PcomY* dataset, given the sequestration model. Using those parameters, we then generated a simulation of the *PcomY* versus *PcomX* activity. We compared these results to the experimental data for the $\Delta clpC$ strain.

In plotting the simulation (Fig. 6), we modeled the weak red auto-fluorescence background in the data by adding baseline Gaussian noise of 3 ± 0.8 red fluorescence units; this baseline is small compared to the typical red fluorescence ($\sim 10^2 - 10^4$ units) of *comY* activated cells.

Acknowledgements

The authors thank Momin Haider for collecting the data in Supporting Fig. S4D. This work was supported by 1R01 DE023339, DE13239 and T90 DE021990 from the National Institute of Dental and Craniofacial Research.

References

- Bevis, B.J., Glick, B.S. (2002) Rapidly maturing variants of the *Discosoma* red fluorescent protein (DsRed). *Nat Biotechnol* **20**: 83.
- Bjornstad, T.J., Havarstein, L.S. (2011) ClpC acts as a negative regulator of competence in *Streptococcus thermophilus*. *Microbiology* **157**: 1676–1684.
- Bose, J.L., Fey, P.D., Bayles, K.W. (2013) Genetic tools to enhance the study of gene function and regulation in *Staphylococcus aureus*. *Appl Environ Microbiol* **79**: 2218–2224.
- Boutry, C., Wahl, A., Delplace, B., Clippe, A., Fontaine, L., Hols, P. (2012) Adaptor protein *MecA* is a negative regulator of the expression of late competence genes in *Streptococcus thermophilus*. *J Bacteriol* **194**: 1777–1788.
- Buchler, N.E., Cross, F.R. (2009) Protein sequestration generates a flexible ultrasensitive response in a genetic network. *Molec Syst Biol* **5**: 272–272.
- Cosloy, S. D., Oishi, M. (1973) Genetic transformation in *Escherichia coli* K12. *Proc Natl Acad Sci U S A* **70**: 84–87.
- De Furio, M., Ahn, S.J., Burne, R.A., Hagen, S.J. (2017) Oxidative stressors modify the response of *Streptococcus mutans* to its competence signal peptides. *Appl Environ Microbiol* **83**: e01345–17.
- Dong, G., Tian, X., Gomez, Z.A., Li, Y. (2014) Regulated proteolysis of the alternative sigma factor SigX in *Streptococcus mutans*: implication in the escape from competence. *Appl Environ Microb* **14**: 183.
- Dubnau, D., Losick, R. (2006) Bistability in bacteria. *Mol Microbiol* **61**: 564–572.
- Dufour, D., Villemin, C., Perry, J.A., Lévesque, C.M. (2016) Escape from the competence state in *Streptococcus mutans* is governed by the bacterial population density. *Molec Oral Microbiol* **31**: 501–514.
- Fontaine, L., Wahl, A., Fléchar, M., Mignolet, J., Hols, P. (2015) Regulation of competence for natural transformation in streptococci. *Infect Genet Evol* **33**: 343–360.
- Friedman, N., Cai, L., Xie, X. S. (2006) Linking stochastic dynamics to population distribution: an analytical framework of gene expression. *Phys Rev Lett* **97**: 168302.
- Grote, J., Krysciak, D., Streit, W.R. (2015) Phenotypic heterogeneity, a phenomenon that may explain why quorum sensing does not always result in truly homogenous cell behavior. *Appl Environ Microbiol* **81**: 5280–5289.
- Guo, Q., Ahn, S., Kaspar, J., Zhou, X., Burne, R. A. (2014) Growth phase and pH influence peptide signaling for

- competence development in *Streptococcus mutans*. *J Bacteriol* **196**: 227–36.
- Hagen, S. J., Son, M. (2017) Origins of heterogeneity in *Streptococcus mutans* competence: interpreting an environment-sensitive signaling pathway. *Phys Biol* **14**: 015001.
- Hossain, M. S., Biswas, I. (2012) An extracellular protease, SepM, generates functional competence-stimulating peptide in *Streptococcus mutans* UA159. *J Bacteriol* **194**: 5886–5896.
- Inobe, T., Matouschek, A. (2008) Protein targeting to ATP-dependent proteases. *Curr Opin Struct Biol* **18**: 43–51.
- Jeon, N.L., Dertinger, S.K.W., Chiu, D.T., Choi, I.S., Stroock, A.D., Whitesides, G.M. (2000) Generation of solution and surface gradients using microfluidic systems. *Langmuir* **16**: 8311–8316.
- Johnston, C., Martin, B., Fichant, G., Polard, P., Claverys, J. (2014) Bacterial transformation: distribution, shared mechanisms and divergent control. *Nat Rev Micro* **12**: 181–196.
- Kirstein, J., Schlothauer, T., Dougan, D.A., Lilie, H., Tischendorf, G., Mogk, A., et al. (2006) Adaptor protein controlled oligomerization activates the AAA+ protein ClpC. *EMBO J* **25**: 1481–1491.
- Kwak, I.H., Son, M., Hagen, S.J. (2012) Analysis of gene expression levels in individual bacterial cells without image segmentation. *Biochem Biophys Res Commun* **421**: 425–430.
- Lauderdale, K.J., Malone, C.L., Boles, B.R., Morcuende, J., Horswill, A.R. (2010) Biofilm dispersal of community-associated methicillin-resistant *Staphylococcus aureus* on orthopedic implant material. *J Orthop Res* **28**: 55–61.
- LeBlanc, D.J., Lee, L.N., Abu-Al-Jaibat, A. (1992) Molecular, genetic, and functional analysis of the basic replicon of pVA380-1, a plasmid of oral streptococcal origin. *Plasmid* **28**: 130–145.
- Lemme, A., Grobe, L., Reck, M., Tomasch, J., Wagner-Dobler, I. (2011) Subpopulation-specific transcriptome analysis of competence-stimulating-peptide-induced *Streptococcus mutans*. *J Bacteriol* **193**: 1863–1877.
- Lemos, J.A.C., Burne, R.A. (2002) Regulation and Physiological Significance of ClpC and ClpP in *Streptococcus mutans*. *Journal of Bacteriology* **184**: 6357–6366.
- Lemos, J.A., Burne, R.A. (2008) A model of efficiency: stress tolerance by *Streptococcus mutans* **154**: 3247–3255.
- Leung, V., Dufour, D., Levesque, C.M. (2015) Death and survival in *Streptococcus mutans*: differing outcomes of a quorum-sensing signaling peptide. *Front Microbiol* **6**: 1176.
- Leung, V., Ajdic, D., Koyanagi, S., Lévesque, C. M. (2015) The formation of *Streptococcus mutans* persists induced by the quorum-sensing peptide pheromone is affected by the LexA regulator. *J Bacteriol* **197**: 1083–1094.
- Li, Y. H., Tian, X. (2017) Proteolytic regulation of competence development in the genus streptococcus: implications in competence, stress response and antibacterial therapy. *J Antimicrob Agents* **3**: 148.
- Li, Y., Lau, P., Lee, J., Ellen, R., Cvitkovitch, D. (2001) Natural genetic transformation of *Streptococcus mutans* growing in biofilms. *J Bacteriol* **183**: 897–908.
- Liu, J., Mei, Z., Li, N., Qi, Y., Xu, Y., Shi, Y., et al. (2013) Structural dynamics of the MecA-ClpC complex: A Type II AAA+ protein unfolding machine. *J Biol Chem* **288**: 17597–17608.
- Mashburn-Warren, L., Morrison, D.A., Federle, M.J. (2010) A novel double-tryptophan peptide pheromone controls competence in *Streptococcus* spp. via an Rgg regulator. *Mol Microbiol* **78**: 589–606.
- Mei, Z., Wang, F., Qi, Y., Zhou, Z., Hu, Q., Li, H., et al. (2009) Molecular determinants of MecA as a degradation tag for the ClpCP protease. *J Biol Chem* **284**: 34366–34375.
- Merritt, J., Qi, F., Shi, W. (2005) A unique nine-gene *comY* operon in *Streptococcus mutans*. *Microbiology* **151**: 157–166.
- Moye, Z.D., Son, M., Rosa-Alberty, A.E., Zeng, L., Ahn, S., Hagen, S.J., et al. (2016) Effects of carbohydrate source on genetic competence in *Streptococcus mutans*. *Appl Environ Microbiol* **82**(15): 4821–4834.
- Perry, J. A., Cvitkovitch, D.G., Levesque, C.M. (2009) Cell death in *Streptococcus mutans* biofilms: a link between CSP and extracellular DNA. *FEMS Microbiol Lett* **299**: 261–266.
- Radeck, J., Kraft, K., Bartels, J., Cikovic, T., Dur, F., Emenegger, J., et al. (2013) The Bacillus BioBrick Box: generation and evaluation of essential genetic building blocks for standardized work with *Bacillus subtilis*. *J Biol Eng* **7**: 29.
- Reck, M., Tomasch, J., Wagner-Döbler, I. (2015) The alternative sigma factor SigX controls bacteriocin synthesis and competence, the two quorum sensing regulated traits in *Streptococcus mutans*. *PLoS Genet* **11**: e1005353.
- Rotem, E., Loinger, A., Ronin, I., Levin-Reisman, I., Gabay, C., Shores, N., et al. (2010) Regulation of phenotypic variability by a threshold-based mechanism underlies bacterial persistence. *Proc Natl Acad Sci* **107**: 12541–12546.
- Seaton, K., Ahn, S., Sagstetter, A.M., Burne, R.A. (2011) A transcriptional regulator and ABC transporters link stress tolerance, (p)ppGpp, and genetic competence in *Streptococcus mutans*. *J Bacteriol* **193**: 862–874.
- Shanker, E., Federle, M.J. (2016) Quorum sensing regulation of competence and bacteriocins in *Streptococcus pneumoniae* and *mutans*. *Genes* **8**: 15.
- Shields, R.C., Burne, R.A. (2016) Growth of *Streptococcus mutans* in biofilms alters peptide signaling at the sub-population level. *Front Microbiol* **7**: 1075.
- Sia, S.K., Whitesides, G.M. (2003) Microfluidic devices fabricated in poly(dimethylsiloxane) for biological studies. *Electrophoresis* **24**: 3563–3576.
- Smith, E.G., Spatafora, G.A. (2012) Gene regulation in *S. mutans*. *J Dent Res* **91**: 133–141.
- Smits, W.K., Kuipers, O.P., Veening, J. (2006) Phenotypic variation in bacteria: the role of feedback regulation. *Nat Rev Micro* **4**: 259–271.
- Son, M., Shields, R., Ahn, S.J., Burne, R.A., Hagen, S.J. (2015) Bidirectional signaling in the competence regulatory pathway of *Streptococcus mutans*. *FEMS Microbiol Lett* **362**: fnv159.
- Son, M., Ahn, S., Guo, Q., Burne, R.A., Hagen, S.J. (2012) Microfluidic study of competence regulation in *Streptococcus mutans*: environmental inputs modulate bimodal and unimodal expression of *comX*. *Mol Microbiol* **86**: 258–272.

- Son, M., Ghoreishi, D., Ahn, S., Burne, R.A., Hagen, S.J. (2015) Sharply tuned pH response of genetic competence regulation in *Streptococcus mutans*: A microfluidic study of environmental sensitivity of *comX*. *Appl Environ Microb* **81**: 5622–5631.
- Taniguchi, Y., Choi, P.J., Li, G., Chen, H., Babu, M., Hearn, J., et al. (2010) Quantifying *E. coli* proteome and transcriptome with single-molecule sensitivity in single cells. *Science* **329**: 533–538.
- Terleckyj, B., Willett, N.P., Shockman, G.D. (1975) Growth of several cariogenic strains of oral streptococci in a chemically defined medium. *Infect Immun* **11**: 649–655.
- Tian, X., Dong, G., Liu, T., Gomez, Z.A., Wahl, A., Hols, P., Li, Y. (2013) MecA protein acts as a negative regulator of genetic competence in *Streptococcus mutans*. *J Bacteriol* **195**: 5196–5206.
- Turgay, K., Hahn, J., Burghoorn, J., Dubnau, D. (1998) Competence in *Bacillus subtilis* is controlled by regulated proteolysis of a transcription factor. *EMBO J* **17**: 6730–6738.
- Turgay, K., Hamoen, L.W., Venema, G., Dubnau, D. (1997) Biochemical characterization of a molecular switch involving the heat shock protein ClpC, which controls the activity of ComK, the competence transcription factor of *Bacillus subtilis*. *Genes Dev* **11**: 119–128.
- Unger, M.A., Chou, H.P., Thorsen, T., Scherer, A., Quake, S.R. (2000) Monolithic microfabricated valves and pumps by multilayer soft lithography. *Science* **288**: 113–116.
- Veening, J., Smits, W.K., Kuipers, O.P. (2008) Bistability, epigenetics, and bet-hedging in bacteria. *Annu Rev Microbiol* **62**: 193–210.
- Wahl, A., Servais, F., Drucbert, A., Foulon, C., Fontaine, L., Hols, P. (2014) Control of natural transformation in salivarius streptococci through specific degradation of sigma-X by the MecA-ClpCP protease complex. *J Bacteriol* **196**: 2807–2816.
- Wang, F., Mei, Z., Qi, Y., Yan, C., Hu, Q., Wang, J., Shi, Y. (2011) Structure and mechanism of the hexameric MecA-ClpC molecular machine. *Nature* **471**: 331–335.
- Zaccaria, E., Wels, M., van Baarlen, P., Wells, J. M. (2016) Temporal regulation of the transformasome and competence development in *Streptococcus suis*. *Front Microbiol* **7**: 1922.
- Zeng, L., Burne, R. A. (2009) Transcriptional regulation of the cellobiose operon of *Streptococcus mutans*. *J Bacteriol* **191**: 2153–2162.

Supporting information

Additional supporting information may be found online in the Supporting Information section at the end of the article.